Dynamics of coupled mode solitons in bursting neural networks

N. Oma Nfor, P. Guemkam Ghomsi, and F. M. Moukam Kakmeni*
Complex Systems and Theoretical Biology Group (CoSTBiG),
Laboratory of Research on Advanced Materials and Nonlinear Science(LaRAMaNS),
Department of Physics, Faculty of Science, University of Buea, P.O. Box 63 Buea-Cameroon

(Received 6 July 2017; revised manuscript received 30 November 2017; published 15 February 2018)

Using an electrically coupled chain of Hindmarsh-Rose neural models, we analytically derived the nonlinearly coupled complex Ginzburg-Landau equations. This is realized by superimposing the lower and upper cutoff modes of wave propagation and by employing the multiple scale expansions in the semidiscrete approximation. We explore the modified Hirota method to analytically obtain the bright-bright pulse soliton solutions of our nonlinearly coupled equations. With these bright solitons as initial conditions of our numerical scheme, and knowing that electrical signals are the basis of information transfer in the nervous system, it is found that prior to collisions at the boundaries of the network, neural information is purely conveyed by bisolitons at lower cutoff mode. After collision, the bisolitons are completely annihilated and neural information is now relayed by the upper cutoff mode via the propagation of plane waves. It is also shown that the linear gain of the system is inextricably linked to the complex physiological mechanisms of ion mobility, since the speeds and spatial profiles of the coupled nerve impulses vary with the gain. A linear stability analysis performed on the coupled system mainly confirms the instability of plane waves in the neural network, with a glaring example of the transition of weak plane waves into a dark soliton and then static kinks. Numerical simulations have confirmed the annihilation phenomenon subsequent to collision in neural systems. They equally showed that the symmetry breaking of the pulse solution of the system leaves in the network static internal modes, sometime referred to as Goldstone modes.

DOI: 10.1103/PhysRevE.97.022214

I. INTRODUCTION

The evolution of cellular and subcellular processes operating on a hierarchy of time scales generates electrical activities in cells. These processes interact nonlinearly to produce complex temporal activities that are crucial for a holistic physiological behavior in a neural network [1–16]. Within this context, coupled systems play an important role. From the biological perspective, coupled oscillators find applications in: insulin secreting cells in the pancreas; pacemaker cells in the heart; neural networks in the brain and spinal cord that control such rhythmic behaviors as chewing, running, and breathing [12–14]. Communication between neurons and other biological oscillators takes place in a myriad of ways. In the study of interactions between biological systems, the physical basis of mechanism that governs the dynamics of coupled oscillators to effectively describe most biophysical processes in neural networks remains poorly understood.

The dynamics of nerve pulse propagation governed by a system of nonlinearly coupled complex Ginzburg-Landau (CCGL) equations provides a suitable platform to study coupled mode waves in neural networks [17]. Nonlinear dissipative media like: biological nerves, chemical reaction and diffusion systems are best modeled by complex Ginzburg-Landau (CGL) equations, which are essential for the understanding of various patterns [18–24]. In such systems, the combined influence of dispersion, self phase modulations, linear and nonlinear gain and loss leads to the propagation of localized solitary pulses [25,26]. Due to its high relevance in coupled systems, the Hindmarsh-Rose (HR) model [27,28], which is sometimes considered as the generalization of the Fitzhugh equations [29], is a good candidate for the investigation of such nonlinearly coupled phenomena. These mathematically simplified systems emanated from the physiological model of Hodgkin-Huxley [30].

The observations of nonlinear excitations and dissipative solitons in neural networks [31,32], have greatly motivated our interest on investigating coupled mode oscillations in such systems. In fact, Moukam Kakmeni *et al.* in Ref. [31] analytically showed that the propagation of modulated waves in neural networks is governed by the modified CGL equation. This was a groundbreaking result because prior to the publication, most scientists could only demonstrate this effect numerically. We believe that, this model can also support coupled modes dynamics, that are modelled by two nonlinearly CCGL equations. By drawing inspiration from the Fermi, Pasta, and Ulam (FPU) observation [33], the lower and upper cutoff modes of wave propagation across the neural network, modeled by the modified CGL equation, are superimposed to analytically check the effects of coupled nonlinearity, which can be considered similar to that of the chemical synaptic coupling.

Because electrical signals are the basis of information transfer in the nervous system, the understanding of neural information processing will require a detailed characterization

*Corresponding author: moukamkakmeni@gmail.com

of how these signals evolve in nerve cells for sensory stimuli and motor commands [1,2]. Coupled mode oscillations incorporates a highly flexible mechanism for neural information processing, thereby providing an elegant tool for information integration across several spatiotemporal coupled neuronal networks [12,34–36]. Experimental data suggest that phase-amplitude coupling in the brain is a superposition of low and high frequency signals [37]. However, this phenomenon is not well understood and will be the subject of the present study. We analyze how strong continuous coupling between lower and upper cutoff modes oscillations influences the dynamics of a neural network, and more importantly, how it impacts on the modes that contain the superposition of the two extreme frequencies in the network. In fact, a neural signal is composed of two distinct components [38–42]: (a) a low-frequency component that is originated primarily by the combined random electrical activities of the neural cells. It is a slow varying signal and it has been shown that this signal conveys some information about the state of rest of the subject under test [43,44]; (b) a high-frequency component called neural spike or action potential that indicates when a neuron generates a short electrical pulse. These spikes are correlated with living beings actions like moving one arm, or associated with some emotions. Thus, a broadband neural signal is the one that contains both low- and high-frequency bands. This is the most interesting signal configuration for neural research, since it preserves all the information of the neural signal [38,42,44]. As, for example, the case of bursting neurons, which are mostly composed of two main frequencies, the burst frequency characterized by the period between two spike in the dynamic state where the neuron repeatedly fires discrete groups (high frequency) and the spiking frequency defined by a period of quiescence before the next burst occurs (low frequency) [27,28,31,45,46].

Note that, common models of nerve signal are based on the one proposed by Hodgkin and Huxley in 1952 [30], who explained that the nerve pulse or action potential is created by a voltage difference across the cell membrane [27–29,31–34,45]. More recently, in 2005, Heimburg and Jackson proposed a new theory saying that nerve signals are sound like density wave [47]. Thus, nerve impulses are due to the lipids of the cell membrane which, at their transition point, are able to generate and propagate a localized short impulse [47]. Following this theory, the problem of collision and annihilation of action potential traveling in opposite directions is very controversial. In fact, in a recent work, A. Gonzalez-Perez *et al.*, reported on collision experiments and indicated that, the collision of two impulses generated simultaneously in orthodromic and antidromic directions, does not result in their mutual annihilation. Instead, they penetrate each other and emerge from the collision without material alterations of their shape or velocity [48]. This result was in agreement with the results on the electromechanical soliton theory for nerve-pulse propagation proposed by Heimburg *et al.* [47]. Nevertheless, this claim was immediately contested by R. W. Berg *et al.* who in a similar experiment, obtained contradictory result [6]. As reported in the literature since more than six decades, action potentials annihilate upon collision [3,5–10,49,50]. In the present study, we also addressed this question from a theoretical and numerical perspective, and the results presented are clearly in agreement with annihilation.

The rest of the work is organized as follows: In Sec. II, from the diffusive HR model we derive the two nonlinearly CCGL equations for the coupled modes. This is achieved by superimposing the lower and upper cutoff modes in the dispersion relation and then applying the multiple scale expansion in a semi-discrete approximation. We explore the modified Hirota method in Sec. III to analytically obtain bright-bright pulse soliton solutions of the nonlinearly CCGL equations. A detailed numerical analysis of the nonlinearly CCGL system is carried out in Sec. IV. A Linear stability analysis in Sec. V shows that the nonlinear coupling favors the instability of plane waves in the neural network. Section VI is devoted to the numerical analysis of the discrete HR system to verify that it supports the analytical solution obtained from the CCGL equation. We end the work with a conclusion in Sec. VII.

II. THE MODEL AND DERIVATION OF THE NONLINEARLY COUPLED EQUATIONS

The Hindmarsh-Rose model for neuronal activity is one of the most widely studied parameterized three-dimensional systems of ordinary differential equations. It arises as a reduction of the conductance-based Hodgkin-Huxley model for neural spiking [27,28]. The model has the capability of exhibiting all qualitatively important and distinct kinds of spiking and bursting behavior. Is arguably the simplest reduction of Hodgkin-Huxley models [30]. In this work, we consider networks of identical Hindmarsh-Rose (HR) neurons symmetrically coupled in a linear way [31,45,46]. The equations governing the evolution of the system are

$$\dot{u}_n = \mu_n - a u_n^3 + b u_n^2 - v_n + I + K(u_{n+1} - 2u_n + u_{n-1}), \tag{1a}$$

$$\dot{\mu}_n = c - d u_n^2 - e\mu_n, \tag{1b}$$

$$\dot{v}_n = r[s(u_n - u_0) - v_n], \tag{1c}$$

where $n = 1,...,N$. The coupling is on the variable u_n, which plays the same role as the membrane potential in a biological neuron. The parameter I plays the role of the input membrane current in a biological neuron. It is capital in determining whether the HR neuron describes various behaviors like quiescent, subthreshold, suprathreshold, or chaotic regime. The variable μ_n accounts for the measure of the rate at which transport of sodium and potassium ions is made through fast ion channels, while v_n is the bursting variable, taking into consideration the rate of the transport of other ions like Cl^- and proteins anions. One of the main roles of this variable is to control the rest period between two action potentials. The variable u_n also defines the activities into the fast subsystem, the variable μ_n is also called spiking variable and the variable v_n defines the activities into the slow subsystem [27,28,31]. The other parameters c, d, and e are constant parameters, and the coupling strength of the gap junction between neurons is represented by K.

To go further with the analysis, the system of Eqs. (1) is transformed as developed in Ref. [31], and we thus obtain the

Liénard form of the diffusive HR model as

$$\ddot{u}_n + \Omega_0^2 u_n + \varepsilon\left(\varepsilon\gamma_0 + \gamma_1 u_n + \varepsilon\gamma_2 u_n^2\right)\dot{u}_n + \varepsilon\lambda_1 u_n^2 + \varepsilon^2\frac{\gamma_2}{3}u_n^3 + \varepsilon^2\lambda_3 v_n = D_0(u_{n+1} - 2u_n + u_{n-1}) + \varepsilon^2 D_1(\dot{u}_{n+1} - 2\dot{u}_n + \dot{u}_{n-1}), \quad (2a)$$

$$\dot{v}_n + r v_n - \Omega_0^2 u_n = 0, \quad (2b)$$

with ε being a perturbation parameter ($\varepsilon << 0$) introduced to take into consideration the order at which each parameter of the coupled system is linked to the slow variable that is maintained into the system, since it defines the bursting behavior important in this analysis. Equation (2a) is therefore the equation regulating the dynamics of the membrane potential in the HR coupled model, and it resembles the one governing the one dimensional dynamics of the potential difference across the cell membrane for a FitzHugh-Nagumo model [51]. Equation (2b) describes the dynamics of the bursting variable, which accounts for the rate at which the transport of some ions such as Cl^- and protein ions is done via slow ions channels.

A. Dispersion relation of wave propagation

There are always frequency limits within which normal propagation of nerve impulse signals are observed across a neural network. Moreover, beyond these limits, the system needs some external perturbations to have stable action potentials. To define the appropriate frequency limit, we employ a perturbation technique where suitable solutions of the diffusive HR model containing the ε parameter are used. Upon substitution of these solutions of the diffusive HR model into Eq. (2), the dispersion relation is obtained with terms at order $\varepsilon^0 e^{i\theta_n}$. In this light, we consider the following solutions of our coupled HR model Eqs. (2):

$$u_n(t) = \varepsilon\phi_n + \psi_n e^{i\theta_n} + \psi_n^* e^{-i\theta_n} + \varepsilon[\rho_n e^{2i\theta_n} + \rho_n^* e^{-2i\theta_n}], \quad (3)$$

$$v_n(t) = \varepsilon G_n + F_n e^{i\theta_n} + F_n^* e^{-i\theta_n} + \varepsilon[H_n e^{2i\theta_n} + H_n^* e^{-2i\theta_n}], \quad (4)$$

with $\theta_n = qn - \omega t$ where q is the normal mode wave number and ω is the angular velocity.

In this semidiscrete approximation ϕ, ψ, ρ (respectively, G, F, H) are supposedly independent of the "fast" variables t and n. Instead, they depend on the "slow" variables defined by $X_i = \varepsilon^i x$ and $T_i = \varepsilon^i t$, for $i \geqslant 1$. A continuum limit approximation is then made with the wave amplitudes while the discrete nature of the phase in maintained. For instance $\psi_n(t)$ is replaced by $\psi(X_1, X_2, ..., T_1, T_2, ...)$, while $\dot{\psi}_n$ and $\psi_{n\pm1}$ are computed at order ε^2 using a Taylor series expansion. Similar expressions hold for ϕ_n, ρ_n, G_n, F_n, and H_n, which are eventually used to evaluate u_n and v_n.

The ansatz considered in both Eqs. (3) and (4) is inherent to the spirit of the multiple-scale expansion method: as the differential operators in space and time domains are expanded over two distinct perturbation scales (though the same perturbation parameter is used, namely ε), the solution too should be expanded. There is no universal order of truncation for this expansion. Usually, the relevant highest-order term in the expansion is determined by the order of expansion of the two differential operators. As elaborated in [31,52], upon substitution of u_n and v_n into Eq. (2a) and collecting terms proportional to $\varepsilon^0 e^{i\theta_n}$, we obtain

$$\psi(-\omega^2) + \psi\Omega_0^2 = D_0[\psi e^{iq} + \psi e^{-iq} - 2\psi],$$

which yields the dispersion relation

$$\omega^2 = \Omega_0^2 + 4D_0 \sin^2\left(\frac{q}{2}\right). \quad (5)$$

From Eq. (5), the linear spectrum has a gap $\omega_{\min} = \Omega_0$ and it is limited by the cutoff frequency $\omega_{\max} = (\Omega_0^2 + 4D_0)^{1/2}$ due to discreteness as shown in Fig. 1.

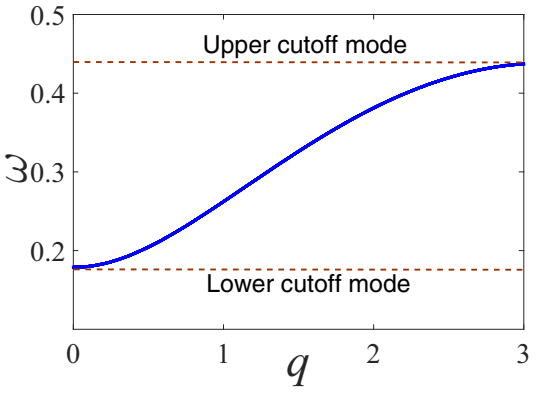

FIG. 1. Linear dispersion curve of the nerve impulse for $D_0 = 0.04$ and $\Omega_0^2 = 0.032$. There is a lower cutoff mode $q = 0$ with frequency $\omega_0 = \Omega_0$ and upper cutoff mode $q = \pi$ with frequency $\omega_{\max} = (\Omega_0^2 + 4D_0)^{1/2}$.

The variation of the diffuseness of the plasma membrane through the parameter D_0, which is the dispersion coefficient, physically accounts for the alteration of ions movement across pumps and ion channels of the neural membranes. This motion of ions coupled with the threshold frequency Ω_0 in Eq. (5), enables us to identify various frequency bands that are unique to specific wave profiles, such as Δ: 1–4 Hz, θ: 4–8 Hz, α: 8–12 Hz, β: 12–30 Hz, and γ: 30–70 Hz [11,53]. A comprehensive neurophysiological mechanism that constrains synchronization to a specific frequency band still remains unclear. However, these oscillations represent ongoing and spontaneous activities of the brain, as exhibited by different neuronal organizations emerging from arrays of neuronal tissues and cells in the brain [54]. In this work, we are interested in a mode that contains the superposition of two extreme frequencies in the system. That is, the lower cutoff mode obtained for $q = 0$ ($\omega_{\min} = \Omega_0$) and the upper cutoff mode obtained when $q = \pi$ ($\omega_{\max} = (\Omega_0^2 + 4D_0)^{1/2}$). Thus, in the following, we will establish the equations describing the nonlinear wave propagation in these modes.

B. Deriving the nonlinearly coupled mode equations

Coupled modes oscillation (CMO) is generally used to study the interdependence between low-frequency and high-frequency neural activities. In the dynamics of real neural networks, larger neural populations oscillate at low frequencies while small neuronal ensembles operate at high frequencies

[55], hence an in-depth knowledge of CMO would enhance flexible coordination of neural activity in the entire network in both spatial and time domains. Moreover, variations in CMO patterns have been shown to be inextricably linked to a myriad of neuronal disorders like Parkinson's disease [56,57], schizophrenia [58,59], and anxiety [60]. Since CMO is ubiquitously observed in most neural networks [13,61,62], it is important to rigorously investigate their effect with the diffusive HR model. The principle behind this coupled-mode system is basically to superimpose the lower and upper cutoff modes. Note that at lower cutoff $\theta_{1n} = q_1 n - \omega_1 t$, where $\omega_1 = \Omega_0$, $q_1 = 0$, and at upper cutoff mode $\theta_{2n} = q_2 n - \omega_2 t$, with $\omega_2 = (\Omega_0^2 + 4D_0)^{1/2}$, $q_2 = \pi$.

To derive the coupled-mode equations from the HR model, we now approximate the solution of Eq. (2) in the form

$$\begin{aligned} u_n(t) = {} & \varepsilon\phi_{1n} + \psi_{1n}\, e^{i\theta_{1n}} + \psi_{1n}^*\, e^{-i\theta_{1n}} \\ & + \varepsilon[\rho_{1n}\, e^{2i\theta_{1n}} + \rho_{1n}^*\, e^{-2i\theta_{1n}}] + \varepsilon\phi_{2n} + \psi_{2n}\, e^{i\theta_{2n}} \\ & + \psi_{2n}^*\, e^{-i\theta_{2n}} + \varepsilon[\rho_{2n}\, e^{2i\theta_{2n}} + \rho_{2n}^*\, e^{-2i\theta_{2n}}], \end{aligned} \tag{6}$$

$$\begin{aligned} v_n(t) = {} & \varepsilon G_{1n} + F_{1n}\, e^{i\theta_{1n}} + F_{1n}^*\, e^{-i\theta_{1n}} \\ & + \varepsilon[H_{1n}\, e^{2i\theta_{1n}} + H_{1n}^*\, e^{-2i\theta_{1n}}] + \varepsilon G_{2n} + F_{2n}\, e^{i\theta_{2n}} \\ & + F_{2n}^*\, e^{-i\theta_{2n}} + \varepsilon[H_{2n}\, e^{2i\theta_{2n}} + H_{2n}^*\, e^{-2i\theta_{2n}}]. \end{aligned} \tag{7}$$

By evaluating the expansion and derivatives of Eqs. (6) and (7) (using multiple scale in the semidiscrete approach), then substituting into Eq. (2a) and collecting terms of order $\varepsilon^0 e^{i\theta_{1n}}$ and $\varepsilon^0 e^{i\theta_{2n}}$, respectively, yields the confirmation of cutoff frequencies ω_1 and ω_2 given above. Terms of order $\varepsilon^1 e^{i\theta_{1n}}$ and $\varepsilon^1 e^{i\theta_{2n}}$, respectively, generate $\frac{\partial \psi_j}{\partial T_1} + v_g \frac{\partial \psi_j}{\partial X_1} = 0$ for $j = 1,2$. But the group velocity v_g vanishes, implying that ψ_j is independent of the time scale T_1. As highlighted in Ref. [31], we collect terms without exponential dependence to have the relation $\phi_j = \frac{-2\lambda_1}{\Omega_0^2}|\psi_j|^2$. Also terms proportional to $\varepsilon^1 e^{2i\theta_{1n}}$ and $\varepsilon^1 e^{2i\theta_{2n}}$ enable us to, respectively, have

$$\rho_1 = \frac{(\lambda_1 - i\omega_1\gamma_1)}{3\Omega_0^2}\psi_1^2, \tag{8a}$$

$$\rho_2 = \frac{(\lambda_1 - i\omega_2\gamma_1)}{3\left(\Omega_0^2 + \frac{16}{3}D_0\right)}\psi_2^2. \tag{8b}$$

We now collect terms of order $\varepsilon^2 e^{i\theta_{1n}}$ and $\varepsilon^2 e^{i\theta_{2n}}$ to, respectively, realize the coupled system of equations:

$$\begin{aligned} \frac{\partial^2\psi_1}{\partial T_1^2} - 2i\omega_1\frac{\partial\psi_1}{\partial T_2} = {} & i\omega_1\gamma_0\psi_1 + (i\omega_1\gamma_1 - 2\lambda_1)(\psi_1\phi_1 + \psi_1^*\rho_1) + (i\omega_1 - 1)\gamma_2|\psi_1|^2\psi_1 \\ & + (2\lambda_1 - i\gamma_2\omega_1)\phi_2\psi_1 + 2\gamma_2(1 - i\omega_1)|\psi_2|^2\psi_1 - \lambda_3 F_1 + D_0\frac{\partial^2\psi_1}{\partial X_1^2}, \end{aligned} \tag{9a}$$

$$\begin{aligned} \frac{\partial^2\psi_2}{\partial T_1^2} - 2i\omega_2\frac{\partial\psi_2}{\partial T_2} = {} & i\omega_2\gamma_0\psi_2 + (i\omega_2\gamma_1 - 2\lambda_1)(\psi_2\phi_2 + \psi_2^*\rho_2) + (i\omega_2 - 1)\gamma_2|\psi_2|^2\psi_2 \\ & + (2\lambda_1 - i\gamma_2\omega_2)\phi_1\psi_2 + 2\gamma_2(1 - i\omega_2)|\psi_1|^2\psi_2 - \lambda_3 F_2 + 4i\omega_2 D_1\psi_2 - D_0\frac{\partial^2\psi_2}{\partial X_1^2}. \end{aligned} \tag{9b}$$

Furthermore, we substitute the expansion and derivatives of Eqs. (6) and (7) into Eq. (2b) and collect the following terms:

Terms proportional to $\varepsilon^0 e^{i\theta_{1n}}$ and $\varepsilon^0 e^{i\theta_{2n}}$, respectively, give

$$F_1 = \frac{\Omega_0^2(r + i\omega_1)}{r^2 + \omega_1^2}\psi_1, \tag{10a}$$

$$F_2 = \frac{\Omega_0^2(r + i\omega_2)}{r^2 + \omega_2^2}\psi_2. \tag{10b}$$

Terms of order $\varepsilon^1 e^{0i\theta_{1n}}$ and $\varepsilon^1 e^{0i\theta_{2n}}$, respectively, yield

$$G_1 = \frac{\Omega_0^2}{r}\phi_1 = -\frac{2\lambda_1}{r}|\psi_1|^2, \tag{11a}$$

$$G_2 = \frac{\Omega_0^2}{r}\phi_2 = -\frac{2\lambda_1}{r}|\psi_2|^2. \tag{11b}$$

Terms of order $\varepsilon^1 e^{2i\theta_{1n}}$ and $\varepsilon^1 e^{2i\theta_{2n}}$, respectively, generate

$$H_1 = \frac{\Omega_0^2(r + 2i\omega_1)}{r^2 + 4\omega_1^2}\rho_1 = \frac{(r + 2i\omega_1)(\lambda_1 - i\omega_1\gamma_1)}{3\left(r^2 + 4\omega_1^2\right)}\psi_1^2, \tag{12a}$$

$$H_2 = \frac{\Omega_0^2(r + 2i\omega_2)}{r^2 + 4\omega_2^2}\rho_2 = \frac{\Omega_0^2(r + 2i\omega_2)(\lambda_1 - i\omega_2\gamma_1)}{\left(r^2 + 4\omega_2^2\right)\left(3\Omega_0^2 + 16D_0\right)}\psi_2^2. \tag{12b}$$

Finally, we simplify the system of Eqs. (9) by substituting the values of ϕ_j, ρ_j, and F_j obtained above to have

$$i\frac{\partial\psi_1}{\partial T_2} + \frac{P_1}{2}\frac{\partial^2\psi_1}{\partial X_1^2} + [Q_1|\psi_1|^2 + C_1|\psi_2|^2]\psi_1 + i\frac{R_1}{2}\psi_1 = 0, \tag{13a}$$

$$i\frac{\partial\psi_2}{\partial T_2} + \frac{P_2}{2}\frac{\partial^2\psi_2}{\partial X_1^2} + [Q_2|\psi_2|^2 + C_2|\psi_1|^2]\psi_2 + i\frac{R_2}{2}\psi_2 = 0, \tag{13b}$$

which is a system of two nonlinearly CCGL equations. The coefficients P_1, P_2, Q_1, Q_2, C_1, C_2, R_1, and R_2 are given in Appendix A, with the dispersion coefficients P_1, P_2 being purely real. Q_1, Q_2 are the complex self-phase modulation (SPM) coefficients, while R_1, R_2 are the complex dissipative coefficients that account for the linear gain or loss. Last, C_1, C_2 are the nonlinear coupling coefficients responsible for cross-phase modulation (XPM) and essentially affecting the symmetry-breaking transformations of bright solitons [63].

For $C_1 = C_2 = 0$, we obtain the uncoupled complex Ginzburg-Landau (CGL) equations. Generally speaking, the CGL equation is one of the most-studied nonlinear equations in the physics world today. This is because it gives a qualitative and quantitative description of a myriad of physical activities [18,31,64]. In neural networks, the observed propagation of modulated nerve impulse is governed by the CGL equation, which clearly demonstrates how neurons participate in the processing and sharing of information [31]. Exact analytical solutions for solitary pulses in models based on CGL equations have already been obtained using a variety of techniques [17–22]. Depending on the nonlinear interaction coefficients C_j, two forms of wave emerge: standing stable plane waves or traveling waves. Beside these waves, one can also observe amplitude death, complex localized pattern, and spatiotemporal chaos for different values of C_j.

This nonlinearly CCGL system Eq. (13), finds applications in many fields of coupled mode analysis. In the context of hydrodynamics, it can be used to model the interaction of counter-propagating waves under convection in binary-fluids [65–70]. It is also prominent in oscillatory media [17] and plasma physics [71] among many others. The usage of these coupled mode equations in optics stands tall in a class of its own. This is especially the case with the transition from single-mode to multi-mode propagation of signals in fibers [72,73]. In our present investigation with nerve impulse propagation, it mainly describes the activities at lower and upper cutoff modes. Such multimode dynamics due to nonlinear coupling has the potentials of distorting, filtering and stabilizing neural impulse signals. Typically, two modes are always associated with the first and second mode envelopes given by $\psi_1(X_1,T_2)$ and $\psi_2(X_1,T_2)$, respectively.

III. ANALYTIC SOLUTION OF THE NONLINEARLY COUPLED MODES EQUATION

It is now incumbent on us to find exact analytical solutions of ψ_1 and ψ_2 in Eq. (13) for $C_j \neq 0$. This can effectively be achieved by using a special method initially introduced by Hirota in 1971 [74].

A. The Modified Hirota operator and its applications

Hirota developed a method for solving nonlinear equations without requiring the complex technique of inverse scattering method. Concretely, the principle of the Hirota bilinear method lies on the implementation of the Hirota bilinear operator, which transforms the nonlinear evolution equations into several coupled bilinear equations. This act decomposes the original complicated equation into a series of relatively simple equations [75,76]. Depending on the nature of the physical problem, several modifications and improvements are made to obtain an even larger class of nonlinear waves.

To solve the nonlinearly CCGL Eq. (13), we use the modified Hirota derivative proposed by Gholam-Ali *et al.* in Ref. [77], and define

$$\begin{aligned}\left(D_x^m D_t^n\right)(G.F) = &\left[\frac{\partial}{\partial x} - \left(\frac{1}{2} + i\alpha_j\right)\frac{\partial}{\partial x'}\right]^m \\ &\times \left[\frac{\partial}{\partial t} - \left(\frac{1}{2} + i\alpha_j\right)\frac{\partial}{\partial t'}\right]^n \\ &\times G(x,t)F(x',t')\Big|_{x=x',t=t'},\end{aligned} \tag{14}$$

$$\Lambda_j(F.F) = \left(\frac{1}{2} + i\alpha_j\right)\left(\frac{3}{2} + i\alpha_j\right)\left(FF_{xx} - F_x^2\right), j = 1,2, \tag{15}$$

where m and n are positive integers and α_j with $j = 1,2$ are real parameters.

We consider the transformations $\psi_j(x,t) = \Psi_j(x,t)\exp(-iR_{ji}/2\ t)$, $P_j' = P_j/2, \Gamma_j = -R_{jr}/2$, $j = 1,2$, and set $T_2 = t$, $X_1 = x$, and use it to rewrite Eq. (13) as

$$i\frac{\partial\Psi_1}{\partial t} + P_1'\frac{\partial^2\Psi_1}{\partial x^2} + [Q_1|\Psi_1|^2 + C_1|\Psi_2|^2]\Psi_1 = i\Gamma_1\Psi_1, \tag{16a}$$

$$i\frac{\partial\Psi_2}{\partial t} + P_2'\frac{\partial^2\Psi_2}{\partial x^2} + [Q_2|\Psi_2|^2 + C_2|\Psi_1|^2]\Psi_2 = i\Gamma_2\Psi_2. \tag{16b}$$

The real coefficients P_1' and P_2' are the dispersion terms that measure the diffusion of ions across the membrane. The real parts of the complex coefficients Q_j and C_j account for the self and cross-phase modulations, respectively, while the imaginary parts measure the nonlinear gain/loss. The linear gain/loss of the coupled modes system is given by the real coefficients Γ_1 and Γ_2.

To apply the modified Hirota method, we perform the following transformations to the system of Eqs. (16):

$$\Psi_1 = \frac{\eta G\exp[i(k_1x - \Omega_1t)]}{F^{\frac{1}{2}+i\alpha_1}},\ \Psi_2 = \frac{\mu H\exp[i(k_2x - \Omega_2t)]}{F^{\frac{1}{2}+i\alpha_2}}. \tag{17}$$

Here, k_1 and k_2 are the wave numbers of the envelopes, Ω_1 and Ω_2 are the angular frequencies of the envelopes. The wave numbers and the angular frequencies are not necessarily interdependent, and $F(x,t)$, $G(x,t)$ and $H(x,t)$ are assumed to be real-valued functions while $\eta = \eta_r + i\eta_i$ and $\mu = \mu_r + i\mu_i$ are complex numbers.

We substitute Eq. (17) into Eq. (16) and apply the modified Bekki-Nozaki Hirota operators Eqs. (14) and (15) to have the

system of equations:

$$\left[\Gamma_1 + \iota_1 - iP_1'k_1^2 + i\Omega_1 - D_{\alpha_1,t} - 2k_1P_1'D_{\alpha_1,x} + iP_1'D_{\alpha_1,x}^2\right](G.F) = 0, \tag{18a}$$

$$[\iota_1 + iP_1'\Lambda_1](F.F) + [(Q_{1i} - iQ_{1r})|\eta|^2G^2 + (C_{1i} - iC_{1r})|\mu|^2H^2] = 0, \tag{18b}$$

$$\left[\Gamma_2 + \iota_2 - iP_2'k_2^2 + i\Omega_2 - D_{\alpha_2,t} - 2k_2P_2'D_{\alpha_2,x} + iP_2'D_{\alpha_2,x}^2\right](H.F) = 0, \tag{18c}$$

$$[\iota_2 + iP_2'\Lambda_2](F.F) + [(Q_{2i} - iQ_{2r})|\mu|^2H^2 + (C_{2i} - iC_{2r})|\eta|^2G^2] = 0, \tag{18d}$$

where the normalization condition $F/|F|^{(\frac{1}{2}+i\alpha_j)} = 1$ is used and ι_j with $j = 1,2$ stand for decoupling constants.

B. Pulse-typed soliton solutions

To look for a pulse-typed soliton solutions of Eqs. (16), functions G, H, and F are assumed to have the following forms:

$$G = \exp\tfrac{1}{2}(Rx + \omega t), \quad H = \exp\tfrac{1}{2}(Rx + \omega t),$$
$$F = 1 + b\exp(Rx + \omega t) + L\exp 2(Rx + \omega t). \tag{19}$$

Equating the proper powers of the exponentials and neglecting higher harmonic terms of the order $\exp 3(Rx + \omega t)$ above, lead to the following relations:

$$\Omega_1 = -\frac{R^2P_1'}{4} + k_1^2P_1',$$

$$\Omega_2 = -\frac{R^2P_2'}{4} + k_2^2P_2', \; R^2 = \frac{\Gamma_1}{\alpha_1P_1'},$$

$$\omega = -2Rk_1P_1' + 2\Gamma_1, \; k_2 = \frac{Rk_1P_1' - \Gamma_1 + \Gamma_2}{RP_2'},$$

$$|\eta|^2 = \frac{b\left[2\alpha_1C_{1r} + C_{1i}\left(\alpha_1^2 - 3/4\right)\right]\Gamma_1}{\alpha_1(Q_{1i}C_{1r} - Q_{1r}C_{1i})}, \quad \iota_1 = \iota_2 = 0,$$

$$|\mu|^2 = -\frac{b\left[2Q_{1r}\alpha_1 + Q_{1i}\left(\alpha_1^2 - 3/4\right)\right]\Gamma_1}{\alpha_1(Q_{1i}C_{1r} - Q_{1r}C_{1i})}.$$

This pulse solution is subjected to the following constraints

$$\Gamma_2 = \frac{\alpha_2P_2'\Gamma_1}{\alpha_1P_1'}, \; P_2' = \frac{\alpha_2P_1'\left[R\left(4\alpha_1^2 + 1\right) - 8\alpha_1k_1\right]}{\alpha_1\left[R\left(4\alpha_2^2 + 1\right) - 8\alpha_2k_2\right]},$$

$$C_{2r} = bR^2\left(3/4 - \alpha_2^2\right)P_2' - \frac{bR^2P_1'\left[2Q_{1r}\alpha_1 + Q_{1i}\left(\alpha_1^2 - 3/4\right)\right]Q_{2r}}{Q_{1r}C_{1i} - Q_{1i}C_{1r}},$$

$$C_{2i} = 2b\alpha_2R^2P_2' - \frac{bR^2P_1'\left[2Q_{1r}\alpha_1 + Q_{1i}\left(\alpha_1^2 - 3/4\right)\right]Q_{2i}}{Q_{1r}C_{1i} - Q_{1i}C_{1r}}.$$

Finally, we obtain the amplitudes of the solutions of the coupled Eq. (16) as

$$|\Psi_1(x,t)|^2 = \frac{|\eta|^2|e^{(Rx+\omega t)}|}{\left|\left[1 + b\,e^{(Rx+\omega t)} - \frac{b^2}{2}e^{2(Rx+\omega t)}\right]\right|}, \tag{20a}$$

$$|\Psi_2(x,t)|^2 = \frac{|\mu|^2|e^{(Rx+\omega t)}|}{\left|\left[1 + b\,e^{(Rx+\omega t)} - \frac{b^2}{2}e^{2(Rx+\omega t)}\right]\right|}. \tag{20b}$$

Figures 2(a) and 2(d) depict the spatiotemporal evolution of the coupled amplitudes in the neural network, while Figs. 2(b) and 2(e), respectively, give the corresponding contour plots. Last, Figs. 2(c) and 2(f) show the coupled solitary bright-bright amplitudes generated in the spatial domain.

IV. NUMERICAL ANALYSIS OF THE COUPLED MODES AMPLITUDE EQUATION

In this section, we numerically seek for solitary wave solutions to the coupled mode amplitude Eqs. (16). It is noteworthy to recall that small amplitude waves are linear, while large amplitude oscillations are typically nonlinear in nature. As the propagation of action potential takes place through a neural network, two intrinsic properties of the medium, namely nonlinearity and dispersion, may affect the evolution of the nerve impulse. Nonlinearity tends to generate a steeper profile of the nerve impulse while dispersion leans towards flattening it. Generally, in Hamiltonian systems the balance between the effects of nonlinearity and dispersion (or diffraction as the case applies) is responsible for the emergence of solitons. However, real biological neural systems are dissipative in nature, thus rendering the dynamic balance between nonlinearity and dispersion insufficient for the observation of stable nerve impulse. Consequently, we also require the additional balance between

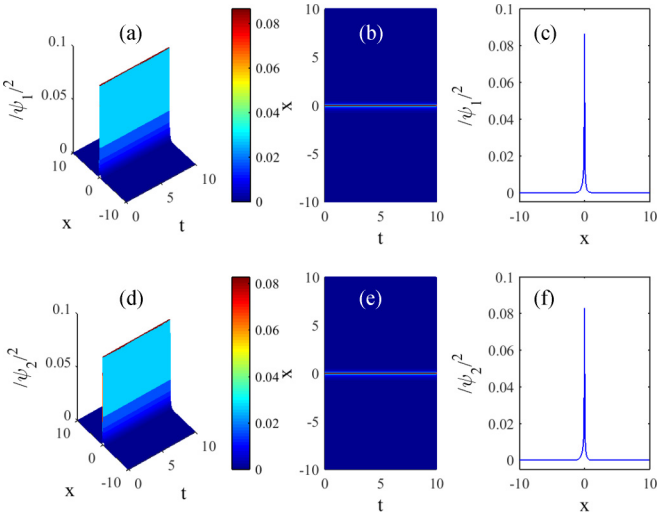

FIG. 2. Spatiotemporal evolution of stationary bright-bright solitary waves of solution Eq. (20) on left column and corresponding contour plot on right column. This is for $P_1' = -0.011$, $Q_1 = 0.7 + 1.2i$, $Q_2 = -1.0 + 0.4i$, $C_1 = -0.5 + 0.6i$, $\Gamma_1 = 0.1$, $\alpha_1 < 0$, $\alpha_2 < 0$. **(a,b)** $|\eta|^2 = 0.338$, $k_1 = -14.0$, $b = 3.0$, $L = 4.5$ **(c,d)** $|\mu|^2 = 0.324$, $k_1 = -14.0$, $b = 3.0$, $L = 4.5$ **(e,f)** $|\eta|^2 = 0.338$, $k_1 = -28.0$, $b = 100.0$, $L = 5.0$ **(g,h)** $|\mu|^2 = 0.324$, $k_1 = -28.0$, $b = 100.0$, $L = 5.0$.

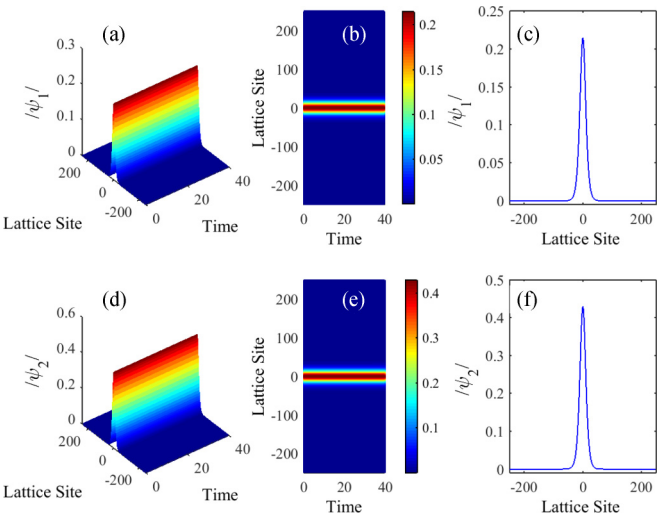

FIG. 3. Dynamics of the lower and upper cutoff modes amplitudes $|\Psi_1|$ and $|\Psi_2|$, respectively, for the coupled system of Eq. (16). The lower and upper cutoff modes $|\Psi_1|$ and $|\Psi_2|$ are both localized (static) bright solitons with: (a) Three-dimensional evolution of $|\Psi_1|$ on all the computational domain, (b) upper view of $|\Psi_1|$, (c) profile of $|\Psi_1|$ at all times; (d) three-dimensional evolution of $|\Psi_2|$ on all the computational domain, (e) upper view of $|\Psi_2|$, (f) profile of $|\Psi_2|$ at all times. The parameter values are taken as: $P_1^{'} = 0.0000011$, $Q_1 = 0.7 + 0.001i$, $C_1 = -0.5$, $\Gamma_1 = 0.0001$, $P_2^{'} = 0.0000011$, $Q_2 = -1.0 + 0.001i$, $C_2 = 0.5$, and $\Gamma_2 = 0.0001$.

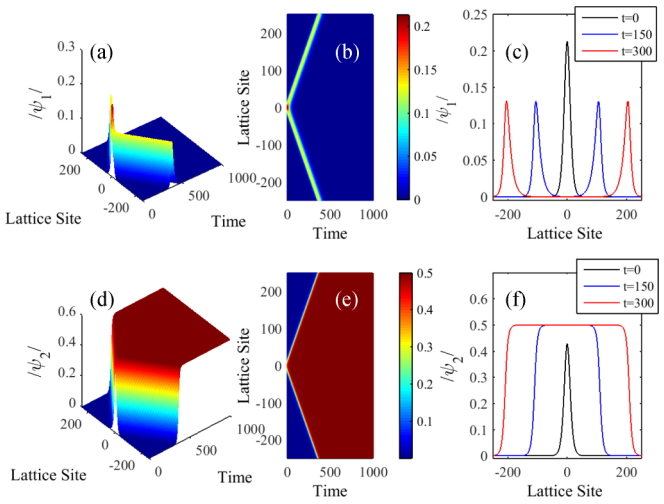

FIG. 4. Dynamics of the lower and upper cutoff modes amplitudes $|\Psi_1|$ and $|\Psi_2|$, respectively, for the coupled system of Eqs. (16). The lower cutoff mode $|\Psi_1|$ is a bisoliton propagating through the medium and the upper cutoff mode $|\Psi_2|$ is a set of two kinks: a kink and an antikink propagating through the medium. (a) Three-dimensional evolution of $|\Psi_1|$ on all the computational domain, (b) upper view of $|\Psi_1|$, (c) profiles of $|\Psi_1|$ at three different times; (d) three-dimensional evolution of $|\Psi_2|$ on all the computational domain, (e) upper view of $|\Psi_2|$, (f) profiles of $|\Psi_2|$ at three different times. The parameter values are taken as: $P_1^{'} = -0.000011$, $Q_1 = 0.7 + 1.2i$, $C_1 = -0.5 + 0.6i$, $\Gamma_1 = 0.1$, $P_2^{'} = -0.000011$, $Q_2 = -0.1 + 0.4i$, $C_2 = -0.5 + 0.6i$, and $\Gamma_2 = 0.1$.

the gain and loss during the process of exchange of ions between the intracellular and extracellular fluids of a neural membrane and also between neighboring cells. Therefore, capturing solitary wave solutions in dissipative systems is a more challenging issue because of this double balance. In some special cases, the effects of dissipation clearly dominates that of linear dispersion, leading to a nonlinear diffusive process because of the interplay between nonlinearity and dissipation. Travelling pulses in dissipative media are some times termed dissipative solitons, and were first predicted to exist in reaction-diffusion systems [78]. In our current investigation, the comforting and motivating factor about this numerical investigation of dissipative soliton solutions is that, when the double balance is achieved, the resultant solitary waves are extremely robust. They represent stable structures in the nonlinear system, that exist far from equilibrium.

Solitons generally remain unchanged during interactions, but suffer only a minor phase shift [79,80]. Consequently, they can be looked upon as modes of the system, used to solve initial-value problems by employing a nonlinear superposition of modes [81]. In Sec. III, we rigorously showed that the nonlinearly coupled system Eq. (16) supports pulse-typed soliton solutions. It is therefore natural for us to consider solution Eq. (20) as the initial condition for our numerical scheme. In the light of this, we perform two main numerical analysis by initially considering the "bell-shaped" hyperbolic secant envelope solution Eq. (20) for both $|\Psi_1|$ and $|\Psi_2|$. Subsequently, we perform a similar analysis using two different ansatzs: a "bell-shaped" hyperbolic secant envelope for $|\Psi_1|$ on one hand, and a weak amplitude plane wane for $|\Psi_2|$ on the other hand. This is achieved by considering a partition of 500 points in a one-dimensional spatial domain $[-L, L]$, with a time step of 0.1 and a spatial step of 0.2. The numerical investigation on the system of coupled partial differential Eqs. (16), is based on the finite difference scheme where we take $L = 50$ and impose periodic boundary conditions.

Starting with two "bell-shaped" hyperbolic secant ansatzs depicted in Fig. 2 as initial conditions, localized (static) solitons solutions can be obtained for both modes $|\Psi_1|$ and $|\Psi_2|$, as shown in Fig. 3. Figures 3(a) and Fig. 3(d) show the three-dimensional spatiotemporal evolution of the lower and upper cutoff modes, respectively, in all the computational domain. Their corresponding upper views are presented in Figs. 3(b) and 3(e), respectively. The related profiles of $|\Psi_1|$ and $|\Psi_2|$ are also highlighted in Figs. 3(c) and 3(f), respectively. These observations clearly reaffirms that the coupled system Eqs. (16) support localized modes.

A further numerical treatment of our problem indicates in Fig. 4 that under suitable parameter conditions, interesting events of excitation propagation can occur. Indeed Fig. 4(a) reveals that, starting from a hyperbolic secant soliton solution, the lower cutoff mode can break down into a bisoliton propagating (in opposite directions) in the spatial domain. An upper view of this phenomenon is depicted in Fig. 4(b). Figure 4(c) supports this fact by showing the profiles of this wave at different propagation times. This clearly reinforces the observation experimentally made in Ref. [82], where the pulse-typed soliton that mimics the action potential eventually degenerate into two axonal propagation in opposite directions. The nonlinear coupling immediately triggers the hyperbolic secant ansatz of the upper cutoff mode $|\Psi_2|$ to evolve into

two propagating kinks. That is, a kink moving toward the left while an antikink migrates to the right as portrayed on Fig. 4(f); with their respective profiles obtained at different values of time. This type of solutions are also termed flat-top solitons as the soliton in the course of time becomes wider and flatter [83]. An upper view of this propagation phenomenon is presented in Fig. 4(e), together with its spatiotemporal evolution in the entire spatial domain shown in Fig. 4(d). Figure 4 clearly stresses the coexistence and propagation of a bisoliton wave for the lower cutoff mode, together with two propagating kinks at the upper cutoff mode. An intense observation of these propagating modes in $|\Psi_1|$ and $|\Psi_2|$ reveals that when reaching the boundary of the medium in the neural network, the bisoliton waves collide and annihilate each other. This has damaging effects on the transmission of neuronal information in the network at lower cutoff mode. By neural information, we mean action potential. Note that, neural information is simply action potential which is the variation of transmembrane voltage, triggered by complex physiological mechanisms controlling the opening and closing of selective ion channels. Each action potential is encoded with specific instruction for effectors organs such as muscles or glands. The action potential is the main signalling mechanism to activate synaptic transmission at axon terminals. In fact, the dynamic structure of electrical activities in the nervous system is information rich, with action potentials considered by most neuroscientists to form the basis of electrical signalling [1–4].

Fortunately, the two propagating kinks at the upper cutoff mode also collide at the boundary of the spatial domain at the same time of bisoliton annihilation. This collision obliterates their structures and gives rise to the emergence of a plane wave with the same amplitude as that of the two kinks [an amplitude which saturates at the value of 0.5 as observed on Fig. 4(f)], which subsequently continues to propagate all through the spatial domain without any alteration. The system supported just the upper cutoff mode after the collision since the lower cutoff mode was completely annihilated. In fact, subsequent to the collision, the amplitude of the lower cutoff mode vanishes. Consequently, Eq. (16a) cancels out, and the HR neural network is now governed by a single (uncoupled) complex Ginzburg-Landau equation as obtained in Ref. [31] while analyzing the single mode equation. This single mode complex Ginzburg-Landau equation has been shown to support stable plane waves [31]. Indeed, these observations typically suggest that, prior to the collision, the information in the neuronal network may be carried by the lower cutoff mode via the propagation of a bisoliton wave, while after the collision, the lower cutoff mode disappears and the information is now relayed by the upper cutoff mode through the propagation of a plane wave. These results are in agreement with the results obtained experimentally by Follmann *et al.* [82] using compartmental axon model. Similar results in other works also indicate that all action potential collisions result in annihilation, and that action potentials traveling in opposite directions never crossed [3,5–10,49,50]. This clearly reinforces the idea of refractory period preventing the crossing of action potential. The action potentials at lower and upper cutoff modes developed in this work further support the conclusion from the Hodgkin-Huxley model [30,82]. Our results also confirm the possibility that neuronal action potentials depicting solitonlike behavior, annihilate during collisions under certain conditions [6,49,50].

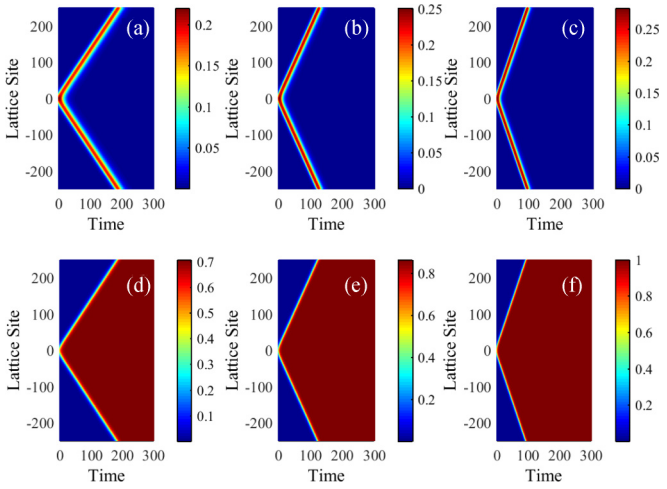

FIG. 5. Effect of the linear gain $\Gamma = \Gamma_1 = \Gamma_2$ on the dynamics of the lower and upper cutoff modes $|\Psi_1|$ and $|\Psi_2|$, respectively, for the coupled system of Eqs. (16). (a, d) $\Gamma = 0.2$, (b, e) $\Gamma = 0.3$, (c, f) $\Gamma = 0.4$. These figures suggest that an increase in the linear gain increases the propagation velocities of the bisoliton and the two-kinks structures. The other parameter values are as on Fig. 4.

Interestingly, Fig. 5 shows the impact of the linear gain on the propagation velocities of both the bisoliton and the two-kinks structures. On this figure, we display the upper views of the propagating coupled modes for different values of the linear gain Γ. For the sake of simplicity and without loss of generality, we assume that $\Gamma_1 = \Gamma_2 = \Gamma$. The most important features highlighted on these figures are the times for which both the bisoliton and the two-kinks waves leave the spatial domain. Figures 5(a) and 5(d) correspond to the upper views of the bisoliton and the two kinks for the value of the linear gain $\Gamma = 0.2$. It is observed that the waves require a propagation time duration slightly above the value of the time $t = 200$, before they can completely leave the neuronal network through its boundaries. Similarly, Figs. 5(b) and 5(e) both correspond to the value of $\Gamma = 0.3$ and show that the propagation time of the waves in this case is strictly found between $t = 150$ and $t = 200$ (i.e., $150 < t < 200$), indicating that the propagating waves are moving faster, as they take a lesser time to completely leave the medium as compared to what was noticed in the case of $\Gamma = 0.2$. A subsequent increase in the linear gain to $\Gamma = 0.4$ shows in Figs. 5(c) and 5(f) that the new total propagation time is strictly found between $t = 100$ and $t = 150$, indicating once more that the wave structures are moving faster than what was observed earlier at the two initial values of $\Gamma = 0.2$ and $\Gamma = 0.3$. At the same time, we observe through the color bars in Fig. 5 that there is a trend that the amplitudes of the different propagating modes also increase with an increase in the linear gain. A confirmation of these facts is highlighted on Fig. 6, where we plot the amplitude [Fig. 6(a)], the total propagation time τ_p [Fig. 6(b)], and the velocity v_p [Fig. 6(c)] of the bisoliton and two-kinks waves as a function of the linear gain Γ. Figure 6(a) shows that as Γ increases, the amplitudes of both the bisoliton

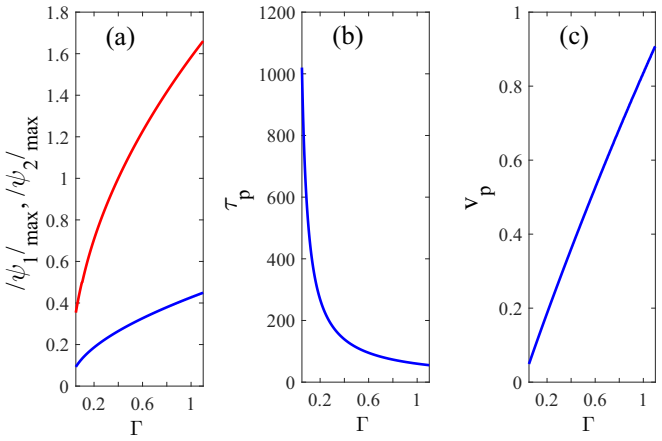

FIG. 6. Effect of the linear gain $\Gamma = \Gamma_1 = \Gamma_2$ on (a) the amplitudes of the bisoliton (in blue) and the two kinks (in red), (b) the total propagation time of both the bisoliton and the two kinks, (c) the propagation velocity of both the bisoliton and the two kinks. The other parameter values are as on Fig. 4.

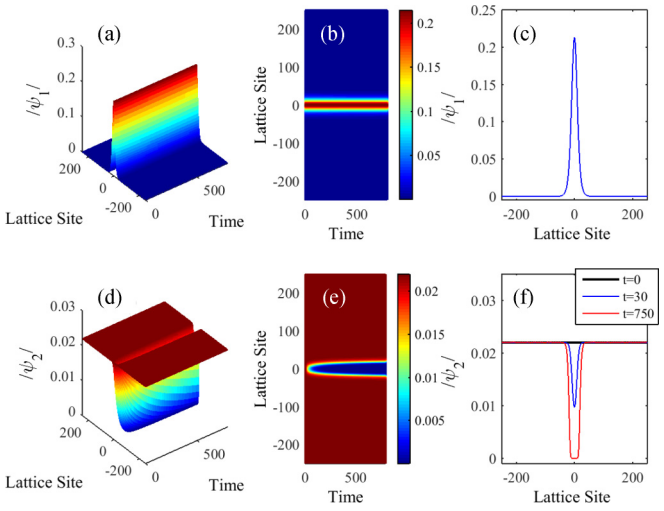

FIG. 7. Dynamics of the lower and upper cutoff modes amplitudes $|\Psi_1|$ and $|\Psi_2|$, respectively, for the coupled system of Eqs. (21). The lower cutoff mode $|\Psi_1|$ is a localized (static) bright soliton and the upper cutoff mode $|\Psi_2|$ is a set of two static kinks: a kink and an antikink emanating from an unstable plane wave and an evanescent dark soliton. (a) Three-dimensional evolution of $|\Psi_1|$ on all the computational domain, (b) upper view of $|\Psi_1|$, (c) profiles of $|\Psi_1|$ at all times; (d) three-dimensional evolution of $|\Psi_2|$ on all the computational domain, (e) upper view of $|\Psi_2|$, (f) profiles of $|\Psi_2|$ at three different times. The parameter values are taken as: $P_1^{'} = 0.000011$, $Q_1 = 0.02 + 0.0001i$, $\Gamma_1 = 0.000001$, $P_2^{'} = 0.000011$, $C_2 = -0.5 + 0.6i$, and $\Gamma_2 = 0.000001$.

(in blue online) and of the two kinks (in red online) increase. Figure 6(b) shows that as Γ increases, the total propagation time of both wave structures decreases tremendously, as a homographic function of the linear gain. This fact is supported by Fig. 6(c) where we observe that as Γ increases, the propagation velocity of both coupled modes increases notably. Therefore, we can conclude that an increase in the linear gain Γ boosts the propagation velocities of both the bisoliton and the two kinks. The rise in the velocities also leads to a corresponding increase in the amplitude of the different soliton structures, hence rendering them to have sharper profiles. Finally, results from Figs. 5 and 6 clearly establish that the linear gain Γ is inextricably linked to the complex electrochemical mechanisms which controls the opening and closing of selective ion channels [30]. It is important to note that the linear gain Γ is directly related to the burst variable of the model. The phenomenological neuron model used here shows that spiking-bursting behavior is of capital importance in the transmissions of information in neural systems since it amplifies the amplitude and the velocity of the action potential, and reduces its propagation time. This is mainly due to the fact that there are many hypotheses on the importance of bursting activity in neural transmission [27,28]. Bursts overcome synaptic transmission failure, facilitate transmitter release, whereas single spikes do not, can be used for selective communication if the postsynaptic cells have subthreshold oscillations of membrane potential, have more informational content than single spikes when analyzed as unitary events [28,31,34].

For the second phase of our numerical analysis, it is crucial to investigate on the condition when the amplitude of the neural signal of one of the modes is very weak compared to the other. For this purpose, we chose the upper cutoff mode to be very weak relative to that at lower cutoff mode. Consequently, the nonlinear term $|\Psi_2|^2$ may be neglected, thereby reducing Eqs. (16) to

$$i\frac{\partial \Psi_1}{\partial T_2} + P_1^{'}\frac{\partial^2 \Psi_1}{\partial X_1^2} + Q_1|\Psi_1|^2\Psi_1 - i\Gamma_1\Psi_1 = 0, \quad (21a)$$

$$i\frac{\partial \Psi_2}{\partial T_2} + P_2^{'}\frac{\partial^2 \Psi_2}{\partial X_1^2} + C_2|\Psi_1|^2\Psi_2 - i\Gamma_2\Psi_2 = 0. \quad (21b)$$

Thus, as it stands, the nonlinearity in the dynamics of the upper cutoff mode $|\Psi_2|$ is therefore induced by the lower cutoff mode via the term $|\Psi_1|^2$. Starting our numerical investigation from a hyperbolic secant ansatz for $|\Psi_1|$ and a small amplitude plane wave for $|\Psi_2|$, we equally observe some remarkable soliton solution structures as depicted in Fig. 7. Under suitable coupling conditions, the lower cutoff mode yields a static bright soliton, whose numerical observation through all the computational domain is shown in Fig. 7(a). Its corresponding upper view and profile are presented in Figs. 7(b) and 7(c), respectively. At the same time, the upper cutoff mode $|\Psi_2|$ evolves as shown in Fig. 7(d). Starting from a weak amplitude plane wave [see black line in Fig. 7(f)], it first evolves towards an unstable dark soliton as depicted in Fig. 7(f) (blue line online). This unstable dark soliton is then in a transient mode because it subsequently collapses into two static kinks as depicted (by the red line online) in Fig. 7(f). An upper cross-sectional view of this phenomenon is shown in Fig. 7(e).

V. STABILITY ANALYSIS OF THE COUPLED MODE EQUATIONS

Stability is a crucial property of a wave profile in a neural network, since it determines whether such a pattern can be observed experimentally, or utilized for diagnostic purposes. Let us recall that the phenomenon of modulational instability results when a steady-state solution is subjected to a weak

perturbation, which eventually leads to its exponential growth along the line of propagation. We investigate the linear stability analysis of constant amplitude coupled modes of Eq. (13) by seeking an equilibrium state of the form $\psi_j = \psi_{j0}e^{i\omega_j t}$. Where $\psi_{j0}, j = 1,2$, is a real constant amplitude and $T_2 \to t$, $X_1 \to x$ for convenience of notation. This gives $\omega_j = Q_j|\psi_{j0}|^2 + C_j|\psi_{l0}|^2 + iR_j/2$, for $j \neq l = 1,2$.

Let us consider a small perturbation around the stationary state defined above by taking [84]

$$\psi_j = (\psi_{j0} + \epsilon_j(x,t))e^{i\omega_j t}, \tag{22}$$

where $\epsilon_j \ll \psi_{j0}$ is a complex number that includes both amplitude and phase corrections. Substituting Eq. (22) in Eq. (13), we obtain the first-order approximation,

$$i\frac{\partial \epsilon_j}{\partial t} + \frac{P_j}{2}\frac{\partial^2 \epsilon_j}{\partial x^2} + Q_j|\psi_{j0}|^2 A_j + C_j\psi_{j0}\psi_{l0}A_l = 0, \tag{23}$$

where $A_j = (\epsilon_j + \epsilon_j^*)$ and $A_l = (\epsilon_l + \epsilon_l^*)$.

Without loss of generality, we set $\Omega_0^2 = \lambda_1$, $\gamma_1 = \gamma_2$ and assume minimal dispersion in the neural network; i.e., $D_0 << \Omega_0^2$. Consequently, the coefficients Q_j and C_j becomes purely real. This is physically acceptable because the effects of the nonlinear gain/loss on the small perturbation ϵ_j around the steady state solution are negligible in the neural network. Upon substitution of $\epsilon_j = \alpha_j' + i\beta_j'$ into Eq. (23), the imaginary part yields

$$\frac{\partial \alpha_j'}{\partial t} + \frac{P_j}{2}\frac{\partial^2 \beta_j'}{\partial x^2} = 0, \tag{24}$$

while the real part gives

$$-\frac{\partial \beta_j'}{\partial t} + \frac{P_j}{2}\frac{\partial^2 \alpha_j'}{\partial x^2} + 2Q_{jr}|\psi_{j0}|^2\alpha_j' + 2C_{jr}\psi_{j0}\psi_{l0}\alpha_l' = 0. \tag{25}$$

The general solution of the linear system Eq. (24) can be obtained analytically by considering the ansatz $\alpha_j' = \alpha_{j0}' \exp[i(k'x - \Omega' t)]$, and we get

$$\beta_j' = -\frac{2i\Omega'}{P_j k'^2}\alpha_j', \tag{26}$$

where Ω' and k' are, respectively, the frequency and propagation constant of the modulated wave.

We now substitute α_j' and β_j' into Eq. (25) to obtain the linearly coupled system,

$$\begin{pmatrix} m_{11} & m_{12} \\ m_{21} & m_{22} \end{pmatrix}\begin{pmatrix} \alpha_{10}' \\ \alpha_{20}' \end{pmatrix} = \begin{pmatrix} 0 \\ 0 \end{pmatrix}, \tag{27}$$

with

$$\begin{aligned} m_{11} &= \frac{2\Omega'^2}{P_1 k'^2} - \frac{P_1 k'^2}{2} + 2Q_{1r}|\psi_{10}|^2, \\ m_{12} &= 2C_{1r}\psi_{10}\psi_{20}, \\ m_{21} &= 2C_{2r}\psi_{20}\psi_{10}, \\ m_{22} &= \frac{2\Omega'^2}{P_2 k'^2} - \frac{P_2 k'^2}{2} + 2Q_{2r}|\psi_{20}|^2. \end{aligned}$$

The dispersion relation is obtained from the solvability condition of the homogeneous matrix Eq. (27), when the determinant of the coefficient matrix vanishes. Finally, we obtain the dispersion relation of the amplitude modulation of the plane wave as

$$\left(\Omega'^2 - \Omega_1'^2\right)\left(\Omega'^2 - \Omega_2'^2\right) = \Omega_{12}'^2\Omega_{21}'^2, \tag{28}$$

where $\Omega_c'^4 = \Omega_{12}'^2\Omega_{21}'^2$, $\Omega_1'^2 = \frac{P_1 k'^2}{2}(\frac{P_1 k'^2}{2} - 2Q_{1r}|\psi_{10}|^2)$, $\Omega_2'^2 = \frac{P_2 k'^2}{2}(\frac{P_2 k'^2}{2} - 2Q_{2r}|\psi_{20}|^2)$, $\Omega_{12}'^2 = P_1 C_{1r}|\psi_{10}|^2 k'^2$, $\Omega_{21}'^2 = P_2 C_{2r}|\psi_{20}|^2 k'^2$.

The dispersion relation Eq. (28) obeys the biquadratic polynomial equation

$$\Omega'^4 - T\Omega'^2 + D = 0, \tag{29}$$

with solution

$$\Omega_\pm'^2 = \tfrac{1}{2}[T \pm (T^2 - 4D)^{1/2}], \tag{30}$$

or

$$\Omega_\pm'^2 = \tfrac{1}{2}\left(\Omega_1'^2 + \Omega_2'^2\right) \pm \tfrac{1}{2}\left[\left(\Omega_1'^2 - \Omega_2'^2\right)^2 + 4\Omega_{12}'^2\Omega_{21}'^2\right]^{1/2}, \tag{31}$$

where $T = \Omega_1'^2 + \Omega_2'^2$ and $D = \Omega_1'^2\Omega_2'^2 - \Omega_{12}'^2\Omega_{21}'^2$. The right-hand side of Eq. (31) is real or complex if the discriminant quantity $\Delta = T^2 - 4D$ is positive or negative, respectively.

For any wave number k', stability is guaranteed if both solutions $\Omega_\pm'^2$ are positive. This is valid provided the conditions $T > 0$, $D > 0$, and $\Delta > 0$ are satisfied.

First, we have that $T = k'^2/2\sum_{j=1}^2 P_j^2(\frac{k'^2}{2} - 2\frac{Q_{jr}}{P_j}|\psi_{j0}|^2)$, where $P_1 > 0$ and $P_2 < 0$. This quantity is positive for any ψ_{j0} and k'. Stability means

$$Q_{2r} > Q_{1r}, \quad Q_{1r} > 0. \tag{32}$$

Second, D is an 8th-order polynomial in k' which can be factorized as $D \sim (k'^4 + b'k'^2 + c')$, where $b' = -4\sum_{j=1}^2 \frac{Q_{jr}}{P_j}|\psi_{j0}|^2$ and $c' = -16\frac{|\psi_{10}|^2|\psi_{20}|^2}{P1P_2}(C_{1r}C_{2r} - Q_{1r}Q_{2r})$ with $b'^2 - 4c' > 0$. For D to be positive (for any value of $k' > 0$ which depicts stability), this implies that $b' > 0$ and $c' > 0$. since $P_1P_2 < 0$, this boils down to

$$C_{1r}C_{2r} - Q_{1r}Q_{2r} > 0. \tag{33}$$

Finally, $\Delta > 0$ is ensured for every value of k' and $|\psi_{j0}|$ provided $P_1P_2C_{1r}C_{2r}|\psi_{10}|^2|\psi_{20}|^2 > 0$. Since $P_1P_2 < 0$, this condition yields

$$C_{1r}C_{2r} < 0. \tag{34}$$

Clearly, conditions Eqs. (32) and (33) are inconsistent with Eq. (34). This shows that the perturbation frequency develops a finite imaginary part and the solution blows up in time. The coupled mode system is therefore modulationally unstable, explaining thus the existence of spatially localized wave profiles. Transmission of neural information by plane waves in the coupled system is therefore very unreliable, as depicted in Fig. 7(f), where the plane waves rapidly degenerates to a dark soliton and then static kinks.

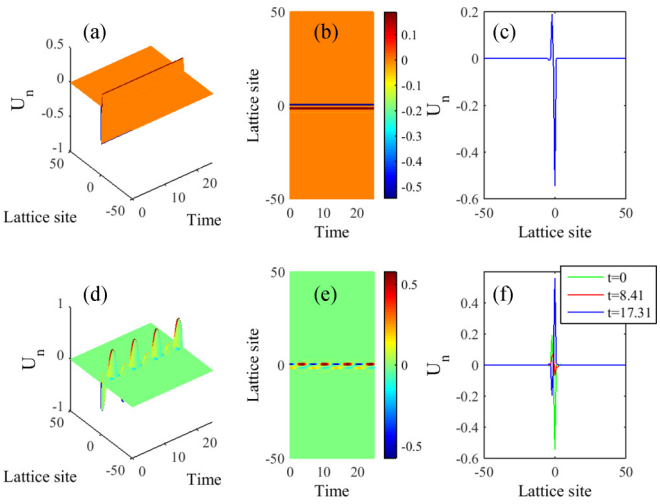

FIG. 8. Membrane (or action) potential solutions of the discrete HR Eqs. (2) in two different parameters conditions. The *upper figures* depict a stationary localized pulse: (a) Three-dimensional view, (b) upper view, (c) profile at all times. The parameters values are: $k_1 = -14.0$, $\Omega_1 = 0.35$, $\omega_1 = 0.179$, $\alpha_1 = 0.15$, $k_2 = -14.0$, $\Omega_2 = 0.35$, $\omega_2 = 0.438$, $\alpha_2 = 0.15$, $r = 0.85202862571$, $\lambda_1 = 0.01$, $\lambda_3 = 0.01$, $\Omega_0^2 = 0.32$, $b = 3.0$, $L = 50$, $R = 3.0$, $\omega = 0.00001061064$, $\gamma_0 = 721.0$, $\gamma_1 = 0.00001$, $\gamma_2 = -0.05$, $D_0 = 0.002$, $D_1 = 0.002$. The *lower figures* depicts a spatially localized standing wave with a time period of about 706 time units: (d) Three-dimensional view, (e) upper view, (f) profiles of the wave at different times. The parameters values are the same as in the *upper figures*, with $\gamma_0 = 0.0$ and $\Omega_0^2 = 1.49$.

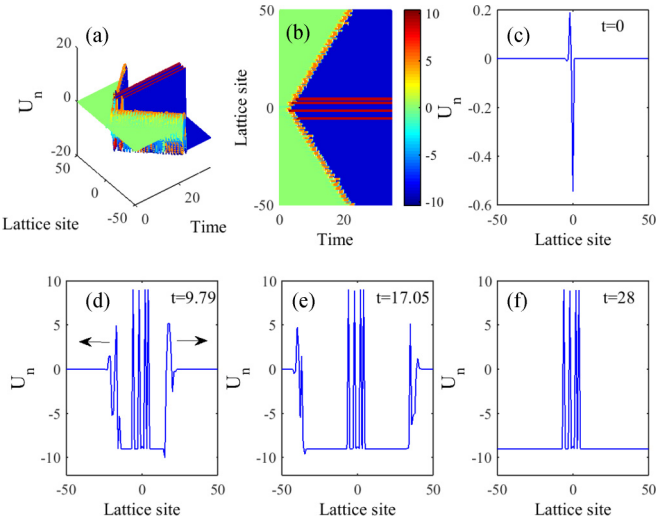

FIG. 9. Membrane (or action) potential solutions of the discrete HR Eqs. (2). The figures depict a Bi-pulse solution traveling in opposite directions, yielding after collision a spatially localized stationary quadripulse or spikes. (a) Three-dimensional view, (b) upper view, (c) profile at all times. The parameters values are the same as in Fig. 8, with $\gamma_0 = 724.0$ and $\Omega_0^2 = 1.49$.

VI. NUMERICAL ANALYSIS OF THE LIENARD FORM OF THE DIFFUSIVE HR MODEL: EXCITABILITY AND COLLISION

The aim of this section is to ascertain the ability of the original HR neuronal network model to support the types of solutions obtained in Sec. IV, as depicted by the numerical treatment of the amplitude equations. For the purpose of this investigation, we integrate the set of Eqs. (2), using the fifth-order Runge-Kutta scheme with a time step of 0.01, on a spatial domain supporting $N = 101$ dynamical units, with periodic boundary conditions. To solve this initial value problem, we take as initial condition the analytical solutions u_n and v_n obtained by using the modified Hirota derivatives and presented as Eqs. (B2) and (B3) in Appendix B. These solutions embed both lower and upper cutoff modes features.

On the upper part of Fig. 8, it is observed that after sending the pulse Ansatz in the system, the structure preserves this excitation state permanently, with no event of propagation, for the given set of the system parameters values. This suggests that stationary localized pulses are accessible for our biological system. This solution is indeed an asymmetric localized solution which intimates the existence of a stable stationary bright envelope soliton solution for our discrete HR model equations. Figures 8(a), 8(b), and 8(c) show, respectively, the three-dimensional spatiotemporal display, the upper view, and the profile of this static pulse solution at all times. It is noteworthy that in other parameter conditions, this pulse solution turns into a localized standing wave with a spatial profile which repeats itself after about 706 time units. Therefore, the temporal period of this standing wave is $T \approx 7.06$. These facts are highlighted on Figs. 8(d), 8(e), and 8(f). Figure 8(f) shows the standing wave profiles at different times.

Interestingly, a further numerical study in other parameters conditions, exhibits scenarios whereby, subsequent to the insertion of the Ansatz, it looses its stability and breaks down into a bipulse (that is two pulses) propagating in opposite directions within the lattice. This phenomenon is observed on Fig. 9. For the given lattice setting, due to the imposed periodic boundary conditions, these two pulses collide at the boundaries of the neuronal lattice and annihilate each other, while leaving in the lattice a stable localized stationary multipulse solution. This multipulse solution is indeed a quadripulse, which can be perceived as being indicative of a localized firing state, with the occurrence of spatially localized static spiking structures in the neuronal network, as shown on Fig. 9(f). These localized static spikes structure in the neural network are well known as static internal modes and are also called Goldstone modes. They are present in any system with a broken continuous symmetry. These Goldstone modes can become the dominant low-energy excitation, showing that symmetry breaking has a profound impact on the physical properties of the HR neural network [85].

The phenomena of wave collision and annihilation depicted in this framework were previously reported in the case of the amplitude equations. Therefore, in agreement with the results derived in Sec. IV, we have shown beyond any reasonable doubt that, our Liénard form of the diffusive HR neuronal model supports coupled modes solutions, with the emergence of a remarkable set of wave phenomena which includes localized stationary pulses, standing waves, bipulse propagation with collision and annihilation events, and the appearance of spatially localized spiking states in the form of multipulse solutions.

VII. CONCLUSION

Communication in a neural network is usually effected by the propagation of action potentials along the fiber of the nerve cells, which has been long thought of as a unidirectional phenomenon. Our current study addressing the crucial issue of multimode propagation of action potentials, where results of the numerical simulations clearly depicts the evolution of action potential in two opposite directions along the nerve axon is of capital importance in the understanding of signal propagation in neural systems. We made use of the axonal multicompartment HR model, where neurons are connected to their nearest neighbors via electrical coupling in a linear chain format. The nonlinearly CCGL equations were later on derived from the Liénard form of the HR model using the multiple scale expansion in the semidiscrete approximation. Such nonlinearly coupled equations elegantly describe the evolution of coupled mode solitons, which are copropagating and interacting with one another in a neural network. We analytically solved the nonlinearly CCGL equations using the modified Hirota bilinear method, which imposes some constraints on the coefficients of the coupled equations. The bright pulse solutions obtained mimic the nerve impulses observed in a neural network, and we believe this study will go a long way to improve the knowledge on coupled modes oscillations in neural networks. Generally, coherent vibrations of coupled oscillatory neural activity result in amplitude changes like the synchronization of membrane potential fluctuations of individual neurons [86]. We observed the propagation of bisolitons in opposite directions at the lower cutoff mode, while the upper cutoff mode supports a kink and an antikink propagation. Upon collision at the boundaries of the network, there is complete annihilation of the bisolitons while the kinks evolve into propagating plane waves. The results suggested that neural information is mainly transmitted at lower cutoff mode by the bisolitons prior to collisions at boundaries. After collision, the transmission of neural information in the coupled system is therefore managed at upper cutoff mode via plane waves. This was a very interesting result because in most systems, neural information is completely lost after collision. The linear gain was also shown to play vital physiological roles during the exchange of ions across membranes. This is because by varying the linear gain Γ, we saw how the speed and profiles of the action potential was greatly modified. The linear stability analysis of the coupled system shows that, it does not support the propagation of stable plane waves. However, It should be noted that during the propagation of stable plane waves in the neural network, only the upper cut off mode existed. That is, the system supported just this mode since the lower cutoff mode was completely annihilated after collision. Interestingly, the numerical analysis of the discrete system confirmed that it supports the solutions obtained in the continuum approximation (CCGL). Numerical simulations also confirmed the annihilation of two pulses colliding at the boundaries of the neuronal lattice, while leaving in the lattice a stable localized stationary multi-pulse solution. This thus demonstrated the robustness of the bisoliton and confirmed the fact that the HR network supports the presence of static internal modes.

ACKNOWLEDGMENT

The authors appreciate the discussions with Emmanuel Yomba of the California State University in USA.

APPENDIX A

$$P_1 = \frac{D_0}{\omega_1},$$

$$P_2 = -\frac{D_0}{\omega_2},$$

$$Q_1 = Q_{1r} + iQ_{1i},$$

$$Q_2 = Q_{2r} + iQ_{2i},$$

$$C_1 = C_{1r} + iC_{1i},$$

$$C_2 = C_{2r} + iC_{2i},$$

$$R_1 = R_{1r} + iR_{1i},$$

$$R_2 = R_{2r} + iR_{2i}.$$

$$Q_{1r} = \frac{10\lambda_1^2 + \omega_1^2\gamma_1^2 - 3\Omega_0^2\gamma_2}{6\omega_1\Omega_0^2},$$

$$Q_{1i} = \frac{\Omega_0^2\gamma_2 - \gamma_1\lambda_1}{2\Omega_0^2},$$

$$Q_{2r} = \frac{1}{2\omega_2}\left[\frac{4\lambda_1^2 - \Omega_0^2\gamma_2}{\Omega_0^2} + \frac{\left(\omega_2^2\gamma_1^2 - 2\lambda_1^2\right)}{3\Omega_0^2 + 16D_0}\right],$$

$$Q_{2i} = \frac{\Omega_0^2\gamma_2 - 2\lambda_1\gamma_1}{2\Omega_0^2} + \frac{3\lambda_1\gamma_1}{6\Omega_0^2 + 32D_0},$$

$$C_{1r} = \frac{\Omega_0^2\gamma_2 - 2\lambda_1^2}{\omega_1\Omega_0^2},$$

$$C_{1i} = \frac{\lambda_1\gamma_2 - \Omega_0^2\gamma_2}{\Omega_0^2},$$

$$C_{2r} = \frac{\Omega_0^2\gamma_2 - 2\lambda_1^2}{\omega_2\Omega_0^2},$$

$$C_{2i} = \frac{\lambda_1\gamma_2 - \Omega_0^2\gamma_2}{\Omega_0^2},$$

$$R_{1r} = \gamma_0 - \frac{\lambda_3\Omega_0^2}{r^2 + \omega_1^2},$$

$$R_{1i} = \frac{r\lambda_3\Omega_0^2}{\omega_1\left(r^2 + \omega_1^2\right)},$$

$$R_{2r} = \gamma_0 + 4D_1 - \frac{\lambda_3\Omega_0^2}{r^2 + \omega_2^2},$$

$$R_{2i} = \frac{r\lambda_3\Omega_0^2}{\omega_2\left(r^2 + \omega_2^2\right)}.$$

APPENDIX B

By using the modified Hirota derivatives, the appropriate solutions of the nonlinearly CCGL system Eq. (13) now reads

$$\psi_1 = F^{-1/2} G(\eta_r + i\eta_i) \exp\Big\{ i(k_1 x - \frac{R_{1i} t}{2} - \Omega_1 t - \alpha_1 \, ln \, F) \Big\}, \tag{B1a}$$

$$\psi_2 = F^{-1/2} H(\mu_r + i\mu_i) \exp\Big\{ i(k_2 x - \frac{R_{2i} t}{2} - \Omega_2 t - \alpha_2 \, ln \, F) \Big\}. \tag{B1b}$$

We now obtain a refined analytic form of the propagating coupled nerve impulse $u_n(t)$ and its corresponding bursting component $v_n(t)$ as

$$\begin{aligned} u_n(t) = {} & \frac{-2\varepsilon\lambda_1}{|F|\Omega_0^2}[G^2 + H^2] + 2F^{-1/2} G \, cos(\Theta_1) + \frac{2\varepsilon}{3\Omega_0^2} F^{-1} G^2 \{\lambda_1 \, cos(2\Theta_1) - \omega_1\gamma_1 \, sin(2\Theta_1)\} \\ & + 2F^{-1/2} H \, cos(\Theta_2) + \frac{2\varepsilon}{3\Omega_0^2 + 16 D_0} F^{-1} H^2 \{\lambda_1 \, cos(2\Theta_2) - \omega_2\gamma_1 \, sin(2\Theta_2)\}, \end{aligned} \tag{B2}$$

$$\begin{aligned} v_n(t) = {} & \frac{-2\varepsilon\lambda_1}{|F| r}[G^2 + H^2] + \frac{2\Omega_0^2}{r^2 + \omega_1^2} F^{-1/2} G\{r \, cos(\Theta_1) - \omega_1 \, sin(\Theta_1)\} \\ & + \frac{2\varepsilon}{3\big(r^2 + 4\omega_1^2\big)} F^{-1} G^2 \Big\{ \big(r\lambda_1 + 2\omega_1^2\gamma_1\big) cos\,(2\Theta_1) - \omega_1(2\lambda_1 - r\gamma_1) sin(2\Theta_1) \Big\} \\ & + \frac{2\Omega_0^2}{r^2 + \omega_2^2} F^{-1/2} H\{r \, cos(\Theta_2) - \omega_2 \, sin(\Theta_2)\} \\ & + \frac{2\varepsilon\Omega_0^2}{\big(r^2 + 4\omega_2^2\big)\big(3\Omega_0^2 + 16 D_0\big)} F^{-1} H^2 \Big\{ \big(r\lambda_1 + 2\omega_2^2\gamma_1\big) \, cos(2\Theta_2) - \omega_2(2\lambda_1 - r\gamma_1) sin(2\Theta_2) \Big\}, \end{aligned} \tag{B3}$$

where

$$\Theta_j = k_j x - \frac{R_{ji} t}{2} - \Omega_j t - \alpha_j \, ln \, F + \theta_{jn}, \; j = 1,2,$$

and without loss of generality, we set $\eta = 1 + 0i$, $\mu = 1 + 0i$ to ease numerical computations. Θ_j can always be transformed back to the original reference coordinates, which contains the ε, n, and t parameters to obtain

$$\Theta_1 = \varepsilon \, k_1 n - \left[\varepsilon^2 \frac{R_{1i}}{2} + \varepsilon^2 \Omega_1 + \omega_1 \right] t - \alpha_1 \, ln \, F, \tag{B4a}$$

$$\Theta_2 = [\varepsilon \, k_2 + \pi] n - \left[\varepsilon^2 \frac{R_{2i}}{2} + \varepsilon^2 \Omega_2 + \omega_2 \right] t - \alpha_2 \, ln \, F. \tag{B4b}$$

This enables us to plot the various spatial profiles of the propagating coupled modes nerve impulses $u_n(t)$ and the bursting variable $v_n(t)$.

[1] D. Purves, G. J. Augustine, D. Fitzpatrick, L. C. Katz, A. LaMantia, J. O. McNamara, and S. M. Williams, *Neuroscience*, 3rd ed. (Sinauer Associates, Massachusetts, 2004).

[2] F. Gabbiani and J. Midtgaard, *Neural Information Processing*, Encyclopedia of Life Sciences (John Wiley & Sons Ltd, New York, 2012),

[3] R. R. Poznanski, L. A. Cacha, Y. M. S. Al-Wesabi, J. Ali, M. Bahadoran, P. P. Yupapin, and J. Yunus, Sci. Rep. **7**, 2746 (2017).

[4] P. A. Rutecki, J. Clin. Neurophysiol. **9**, 195 (1992).

[5] K. El Houssaini, A. I. Ivanov, C. Bernard, and V. K. Jirsa, Phys. Rev. E **91**, 010701(R) (2015).

[6] R. W. Berg, M. T. Stauning, J. B. Sørensen, and H. Jahnsen, Phys. Rev. X **7**, 028001 (2017).

[7] S. Shrivastava, K. H. Kang, and M. F. Schneider, Phys. Rev. E **91**, 012715 (2015).

[8] M. Argentina, P. Coullet, and L. Mahadevan, Phys. Rev. Lett. **79**, 2803 (1997).

[9] X. Li, J. Wang, and W. Hu, Phys. Rev. E **76**, 041902 (2007)

[10] C. D. Acker, N. Kopell, and J. A. White, J. Comput. Neurosci. **15**, 71 (2003).

[11] G. Buzsáki and A. Draguhn, Science **304**, 1926 (2004).

[12] R. T. Canolty and R. T. Knight, Trends Cogn. Sci. **14**, 506 (2010).

[13] A. B. Tort, R. Komorowski, H. Eichenbaum, and N. Kopell, J. Neurophysiol. **104**, 1195 (2010).

[14] A. C. Onslow, R. Bogacz, and M. W. Jones, Progr. Biophys. Molec. Biol. **105**, 49 (2011).

[15] R. J. Field and M. Burger, *Oscillations and Traveling Waves in Chemical Systems* (John Wiley, New York, 1985).

[16] J. D. Robertson, J. Biophys. Biochem. Cytol. **2**, 381 (1956).

[17] Y. Yoshida and Y. Kimura, J. Phys. Soc. Jpn. **78**, 084801 (2009).

[18] Y. Kuramoto, *Chemical Oscillations, Waves, and Turbulence* (Springer, Berlin, 1984).

[19] J. D. Murray, *Mathematical Biology* (Springer, Berlin, 1989).

[20] P. Manneville, *Dissipative Structures and Weak Turbulence* (Academic Press, San Diego, 1990).
[21] R. Kapral and K. Showalter, *Chemical Waves and Patterns* (Kluwer, Doodrecht, 1995).
[22] J. Keener and J. Sneyd, *Mathematical Physiology* (Springer, New York, 1998).
[23] M. C. Cross and P. C. Hohenberg, Rev. Mod. Phys. **65**, 851 (1993).
[24] A. De Wit, Adv. Chem. Phys. **109**, 435 (1999).
[25] N. Akhmediev and A. Ankiewicz, *Dissipative Solitons*, Lecture Notes In Physics, Vol. 661 (Springer, New York, 2004).
[26] N. N. Rosanov, *Spatial Hysteresis and Optical Patterns* (Springer, Berlin, 2002).
[27] J. L. Hindmarsh and R. M. Rose, Nature (London) **296**, 162 (1982).
[28] J. L. Hindmarsh and R. M. Rose, Proc. R. Soc. London, Ser. B **221**, 87 (1984)
[29] R. FitzHugh, Biophys. J. **1**, 445 (1961).
[30] A. L. Hodgkin and A. F. Huxley, J. Physiol. **117**, 500 (1952).
[31] F. M. Moukam Kakmeni, E. M. Inack, and E. M. Yamakou, Phys. Rev. E **89**, 052919 (2014).
[32] A. M. Dikandé and G.-A. Bartholomew, Phys. Rev. E **80**, 041904 (2009).
[33] N. Metropolis, Daedalus **121**, 119 (1992).
[34] G. Ermentrout and N. Kopell, SIAM J. Appl. Math. **46**, 233 (1986).
[35] M. Perez-Armandriz, M. C. Roy, D. C. Spray, and M. V. L. Bennet, Biophys. J. **59**, 76 (1991).
[36] N. Yu, R. Kuske, and Y. X. Li, Chaos **18**, 015112 (2008).
[37] N. J. Kopell, C. Börgers, D. Pervouchine, P. Malerba, and A. B. L. Tort, *Gamma and Theta Rhythms in Biophysical Models of Hippocampal Circuits* (Springer, New York, 2010).
[38] E. R. Kandel, J. H. Schwartz, and T. M. Jessell, *Principles of Neural Science*, 4th ed. (McGraw-Hill Medical, New York, 2000).
[39] L. V. Moran and L. E. Hong, Schiz. Bull. **37**, 659 (2011).
[40] A. Draguhn, R. D. Traub, D. Schmitz, and J. G. R. Jeffreys, Nature **394**, 189 (1998).
[41] C. B. Tabi, A. S. Etemé, and A. Mohamadou, Physica A **474**, 186 (2017).
[42] H. Miranda, V. Gilja, C. A. Chestek, K. V. Shenoy, and T. H. Meng, IEEE Trans Biomed Circuits Syst. **4**, 181 (2010).
[43] G. Santhanam, M. D. Linderman, V. Gilja, S. I. R. A. Afshar, T. H. Meng, and K. V. Shenoy, IEEE Trans. Biomed. Eng. **54**, 2037 (2007).
[44] J. P. Donoghue, J. N. Sanes, N. G. Hatsopoulos, and G. Gaál, J. Neurophysiol. **79**, 159 (1998).
[45] S. Raghavachari and J. A. Glazier, Phys. Rev. Lett. **82**, 2991 (1999).
[46] M. S. Baptista, F. M. M. Kakmeni, and C. Grebogi, Phys. Rev. E **82**, 036203 (2010).
[47] T. Heimburg and A. D. Jackson, Proc. Natl. Acad. Sci. USA **102**, 9790 (2005).
[48] A. Gonzalez-Perez, R. Budvytyte, L. D. Mosgaard, S. Nissen, and T. Heimburg, Phys. Rev. X **4**, 031047 (2014).
[49] J. H. Jennings, D. R. Sparta, A. M. Stamatakis, R. L. Ung, K. E. Pleil, T. L. Kash, and G. D. Stuber, Nature **496**, 224 (2013).
[50] J. Yeomans, Behav. Brain Res. **67**, 121 (1995).
[51] D. T. Bemmo, M. S. Siewe, and C. Tchawoua, Phys. Lett. A **375**, 1944 (2011).
[52] T. Dauxois and M. Peyrard, *Physics of Solitons* (Cambridge University Press, Cambridge, 2006).
[53] P. L. Nunez and R. Srinivasan, *Electric Fields of the Brain: The Neurophysics of EEG* (Oxford University Press, London 1981).
[54] A. Mazaheri and O. Jensen, Front Hum Neurosci. **14**, 177 (2010).
[55] A. Delorme and S. Makeig, J. Neurosci. Methods **134**, 9 (2004).
[56] D. Gabor, J. Inst. Electr. Eng. **93**, 429 (1946).
[57] B. Boashash, Proc. IEEE **80**, 520 (1992).
[58] B. J. He, J. M. Zempel, A. Z. Snyder, and M. E. Raichle, Neuron **66**, 353 (2010).
[59] K. J. Miller, L. B. Sorensen, J. G. Ojemann, and M. den Nijs, PLoS Comput. Biol. **5**, e1000609 (2009).
[60] J. I. Berman, J. McDaniel, S. Liu, L. Cornew, W. Gaetz, T. P. Roberts, and J. C. Edgar, Brain Connect. **2**, 155 (2012).
[61] R. T. Canolty, E. Edwards, S. S. Dalal, M. Soltani, S. S. Nagarajan, H. E. Kirsch, M. S. Berger, N. M. Barbaro, and R. T. Knight, Science **313**, 1626 (2006).
[62] A. F. Rosenberg and M. Ariel, J. Neurophysiol. **63**, 1033 (1990).
[63] H. Sakaguchi and B. A. Malomed, Phys. Rev. E **83**, 036608 (2011).
[64] L. M. Pismen, *Vortices in Nonlinear Fields* (Oxford University/Clarendon Press, Oxford/New York, 1999).
[65] M. C. Cross, Phys. Rev. Lett. **57**, 2935 (1986).
[66] B. A. Malomed, A. A. Nepomnyashchy, and M. I. Tribelsky, Phys. Rev. A **42**, 7244 (1990).
[67] B. A. Malomed, Phys. Rev. E **50**, R3310 (1994).
[68] C. Normand and Y. Pomeau, Rev. Mod. Phys. **49**, 581 (1977).
[69] P. Kolodner, Phys. Rev. A **44**, 6466 (1991).
[70] T. Riste, in *Fluctuations, Instabilities, and Phase Transitions*, Volume 11 of NATO ASI series: Physics, Volume 11 of NATO advanced study institutes series: Physics, NATO, edited by T. Riste (Plenum Press, New York, 1975).
[71] B. Bruhn, Phys. Plasmas **13**, 023505 (2006).
[72] E. Ding, S. Lefrancois, J. N. Kutz, and F. W. Wise, IEEE J. Quant. Electron. **47**, 597 (2011).
[73] J. N. Kutz, B. J. Eggleton, J. B. Stark, and R. E. Slusher, IEEE J. Sel. Topics Quant. Electron. **3**, 1232 (1997).
[74] R. Hirota, Phys. Rev. Lett. **27**, 1192 (1971).
[75] K. Nozaki and N. Bekki, J. Phys. Soc. Jpn. **53**, 1581 (1984).
[76] Tat-Leung Yee, J. Math. Stat. **8**, 413 (2012).
[77] G.-A. Zakeri and E. Yomba, J. Phys. Soc. Jpn. **82**, 084002 (2013).
[78] H. C. Tuckwell, Science **205**, 493 (1979).
[79] S. Trillo, W. E. Torruellas (eds.), *Spatial Solitons* (Springer-Verlag, Berlin, Heidelberg, 2001).
[80] R. Y. Chiao, E. Garmire, and C. H. Townes, Phys. Rev. Lett. **13**, 479 (1964).
[81] V. E. Zakharov and A. B. Shabat, Sov. Phys. JETP **34**, 62 (1972).
[82] R. Follmann, E. Rosa, Jr., and W. Stein, Phys. Rev. E **92**, 032707 (2015).
[83] N. N. Akhmediev, V. V. Afanasjev, and J. M. Soto-Crespo, Phys. Rev. E **53**, 1190 (1996).
[84] I. Kourakis, P. Shukla, and M. Marklund *et al.*, Eur. Phys. J. B **46**, 381 (2005).
[85] S. Hoinka, P. Dyke, M. G. Lingham, J. J. Kinnunen, G. M. Bruun, and C. J. Vale, Nat. Phys. **13**, 943 (2017).
[86] A. Mazaheri and O. Jensen, J. Neurosci. **28**, 7781 (2008).